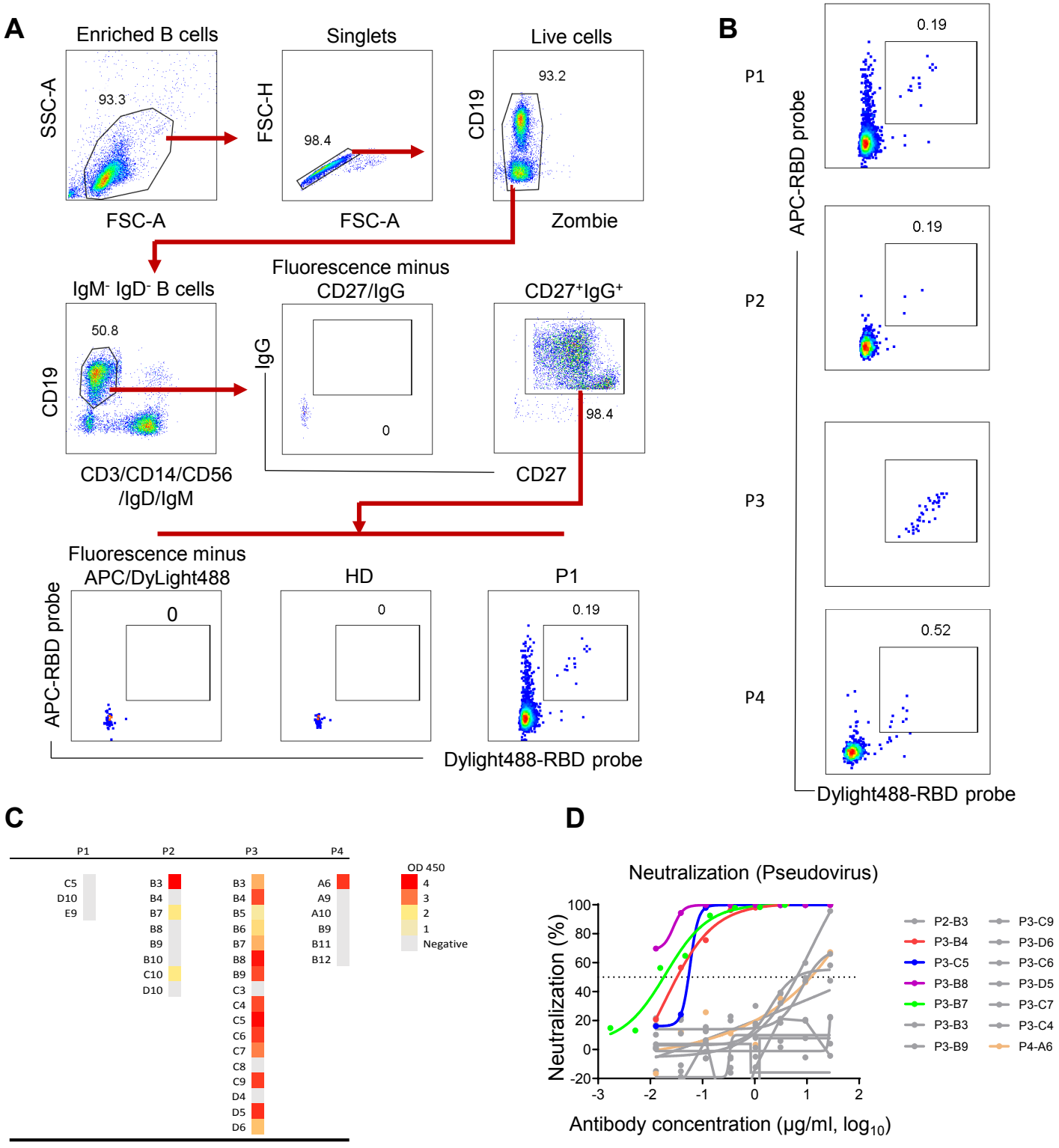

Supplementary Fig. 1. Isolation of SARS-CoV-2 specific antibodies from sorted memory B cells.

(A) The gating strategy for isolation of SARS-CoV-2 RBD-specific memory B cells by flow cytometry.

(B) The RBD double positive cell population was obtained from each subject.

(C) RBD-binding response of individual monoclonal antibodies from 4 subjects by ELISA. The colour scale indicated the absorbance value at OD450 nm.

(D) Neutralization activity was determined for screened antibodies against SARS-CoV-2 pseudovirus. The HuNAbs with high neutralizations were color-coded.

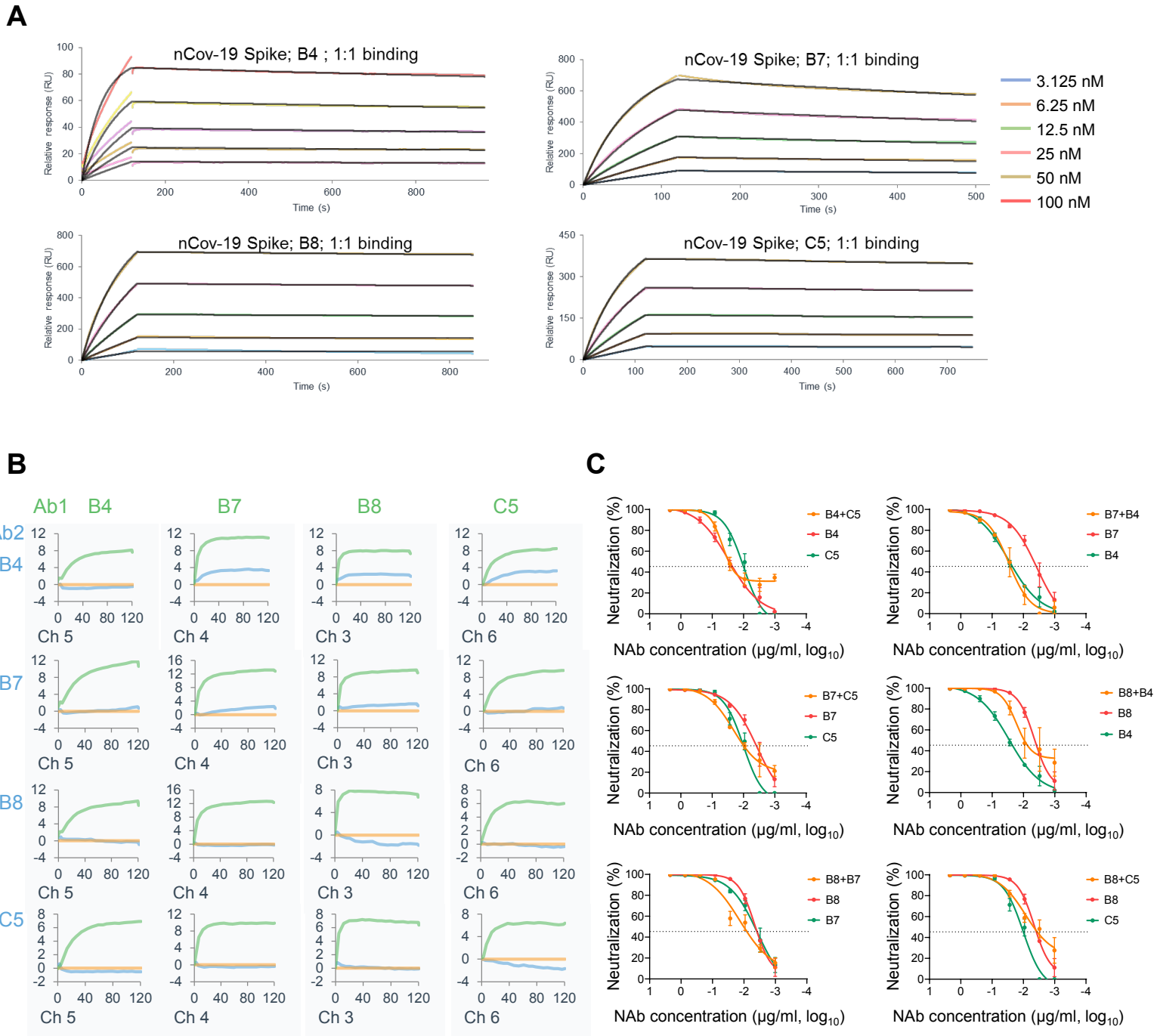

Supplementary Fig. 2. Characterization of purified HuNAbs *in vitro*.
(A) The binding dynamics of four most potent HuNAbs (B4, B7, B8 and C4) to SARS-CoV-2 Spike glycoprotein.
(B) The competitive binding between these four HuNAbs to SARS-CoV-2 RBD. Orange curve: the baseline; Green curve: the binding of test antibody to RBD; Blue Curve: the binding of test antibody (Ab1) to RBD after pre-incubation with the competitor antibody (Ab2).
(C) Lack of synergistic effect between pairs of these four HuNAbs by neutralization assay against the SARS-CoV-2 pseudovirus. The combined antibodies were mixed at 1:1 ratio.

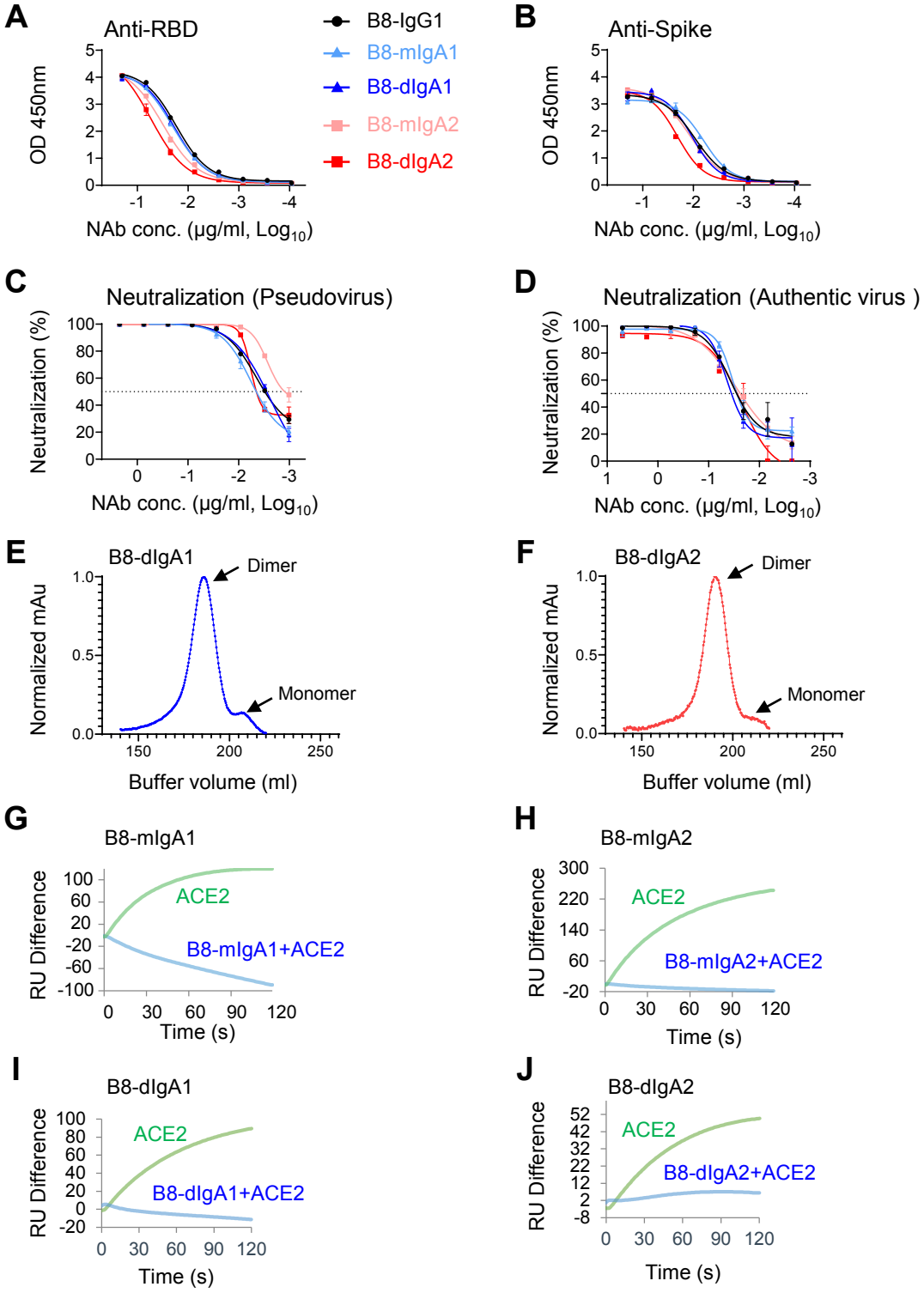

Supplementary Fig. 3. Characterization of B8-based IgA NAbs.
(A) RBD-specific binding activities of B8-mIgA1, B8-mIgA1, B8-dIgA1 and B8-dIgA2 as compared to B8-IgG1 measured by ELISA. **(B)** Spike-specific binding activities of B8-mIgA1, B8-mIgA1, B8-dIgA1 and B8-dIgA2 as compared to B8-IgG1 measured by ELISA. **(C)** Neutralization activities of B8-mIgA1, B8-mIgA1, B8-dIgA1 and B8-dIgA2 as compared to B8-IgG1 measured by decreased pseudotyped SARS-CoV-2 infection in HEK 293T-ACE2 cells. **(D)** Neutralization activities of B8-mIgA1, B8-mIgA1, B8-dIgA1 and B8-dIgA2 as compared to B8-IgG1 measured by decreased authentic SARS-CoV-2 infection in Vero-E6 cells. All the assays above (A-D) were performed in duplicates and the mean of the duplicates was shown with SEM. The antibody concentration in the x-axis is shown in log-transformed units. **(E)** The purity of dimeric B8-dgA1 was confirmed by size exclusion chromatography (SEC). **(F)** The purity of dimeric B8-dgA2 was confirmed by SEC. **(G-J)** The curves show binding of ACE2 to SARS-CoV-2 RBD with (blue) or without (blue) pre-incubation with B8-mIgA1, B8-mIgA2, B8-dIgA1, and B8-dIgA2, respectively, as measured by SPR.

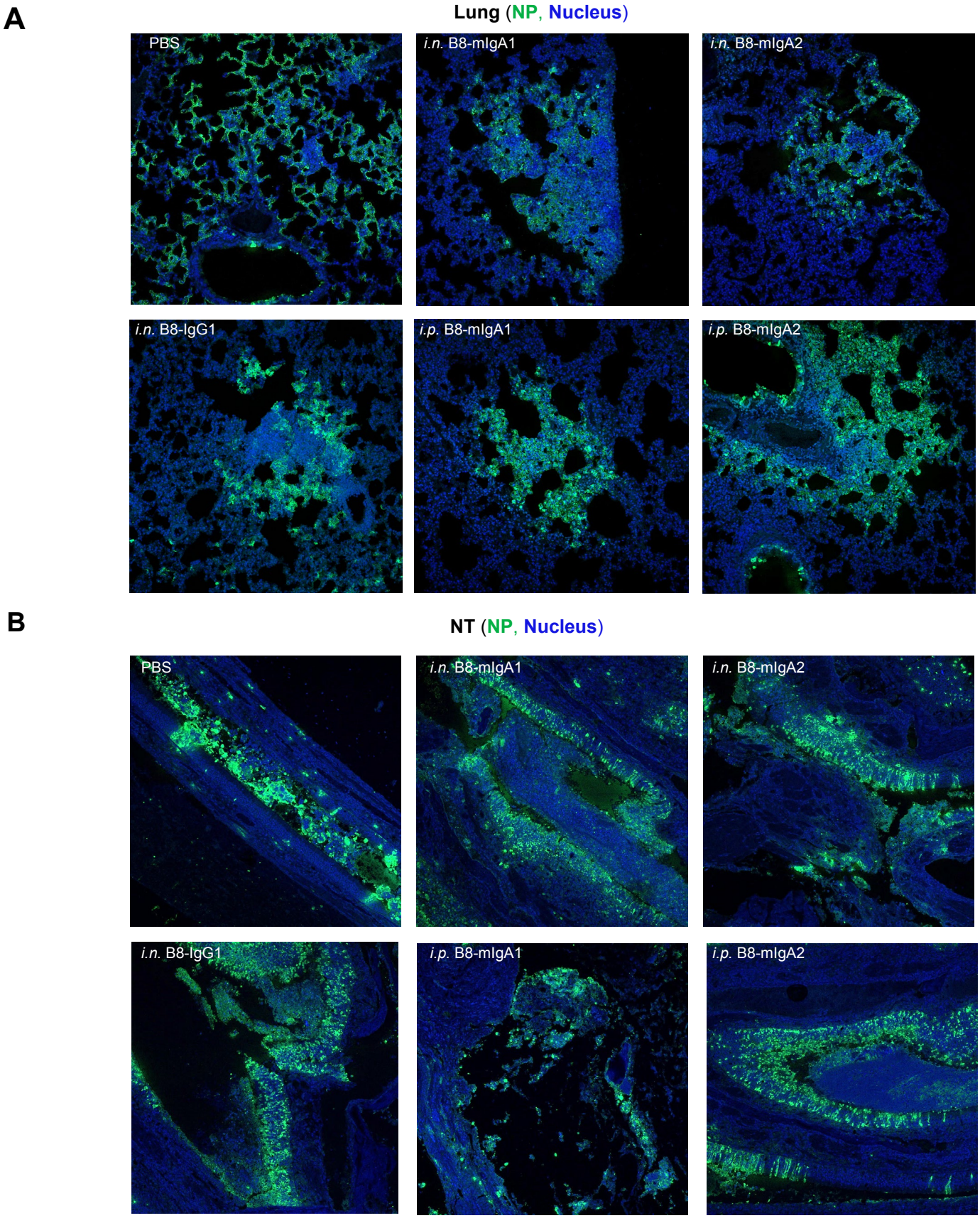

Supplementary Fig. 4. SARS-CoV-2 infection at 4 dpi in both lung and NT of infected Syrian hamsters pre-treated with B8-mIgA1 or B8-mIgA2 by confocal microscope.
(A-B) Representative images (100×) of infected foci in lungs **(A)** and NT **(B)** from each group as determined by anti-NP immunofluorescence (IF) staining. The SARS-CoV-2 NP and cell nuclei were stained with rabbit anti-SARS-CoV-2 NP (green) and DAPI (blue), respectively.

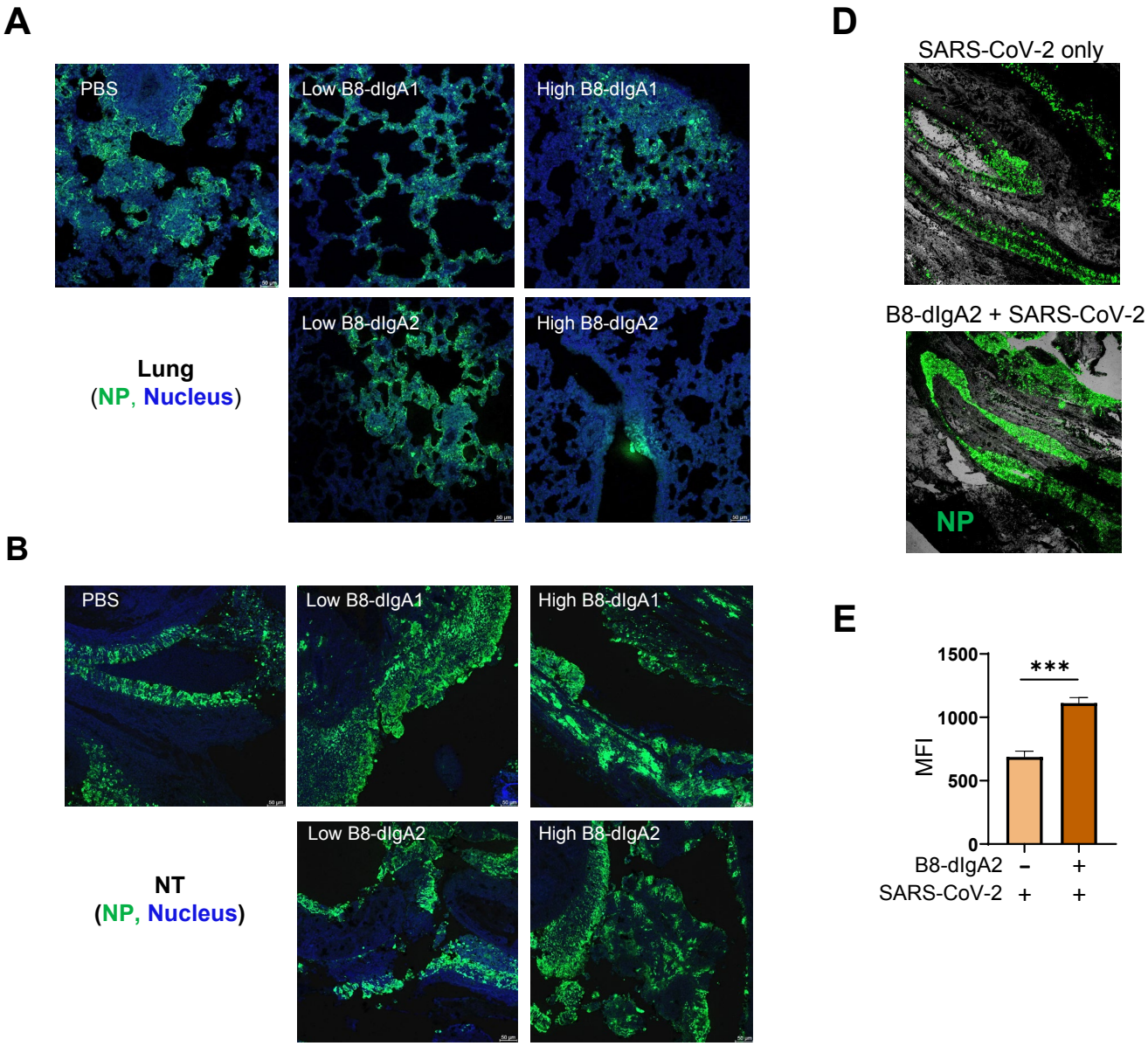

Supplementary Fig. 5. SARS-CoV-2 infection at 4 dpi in both lung and NT of infected Syrian hamsters pre-treated with B8-dIgA1 or B8-dIgA2 by confocal and HE microscope.
(A-B) Representative images (100×) of infected foci in lungs **(A)** and NT **(B)** from each group as determined by anti-NP immunofluorescence (IF) staining. The SARS-CoV-2 NP and cell nuclei were stained with rabbit anti-SARS-CoV-2 NP (green) and DAPI (blue), respectively.
(C) SARS-CoV-2 infection results in more extensive and severe damage of the NT epithelium in B8-dIgA-administrated animals (10× HE images). Injury of the NT epithelium is extensive with partial (black asterisk) or complete (blue asterisk) desquamation in B8-dIgA1- and B8-dIgA2-pretreated Syrian hamsters.
(**D**) Density of NP-positive cells in NT epithelium during live SARS-CoV-2 infection (50× images).
(E) Analysis of NP-positive MFI in 10 random NP-positive areas. Statistics were generated using the student *t* test. *p<0.05; **p<0.01; ***p<0.001.

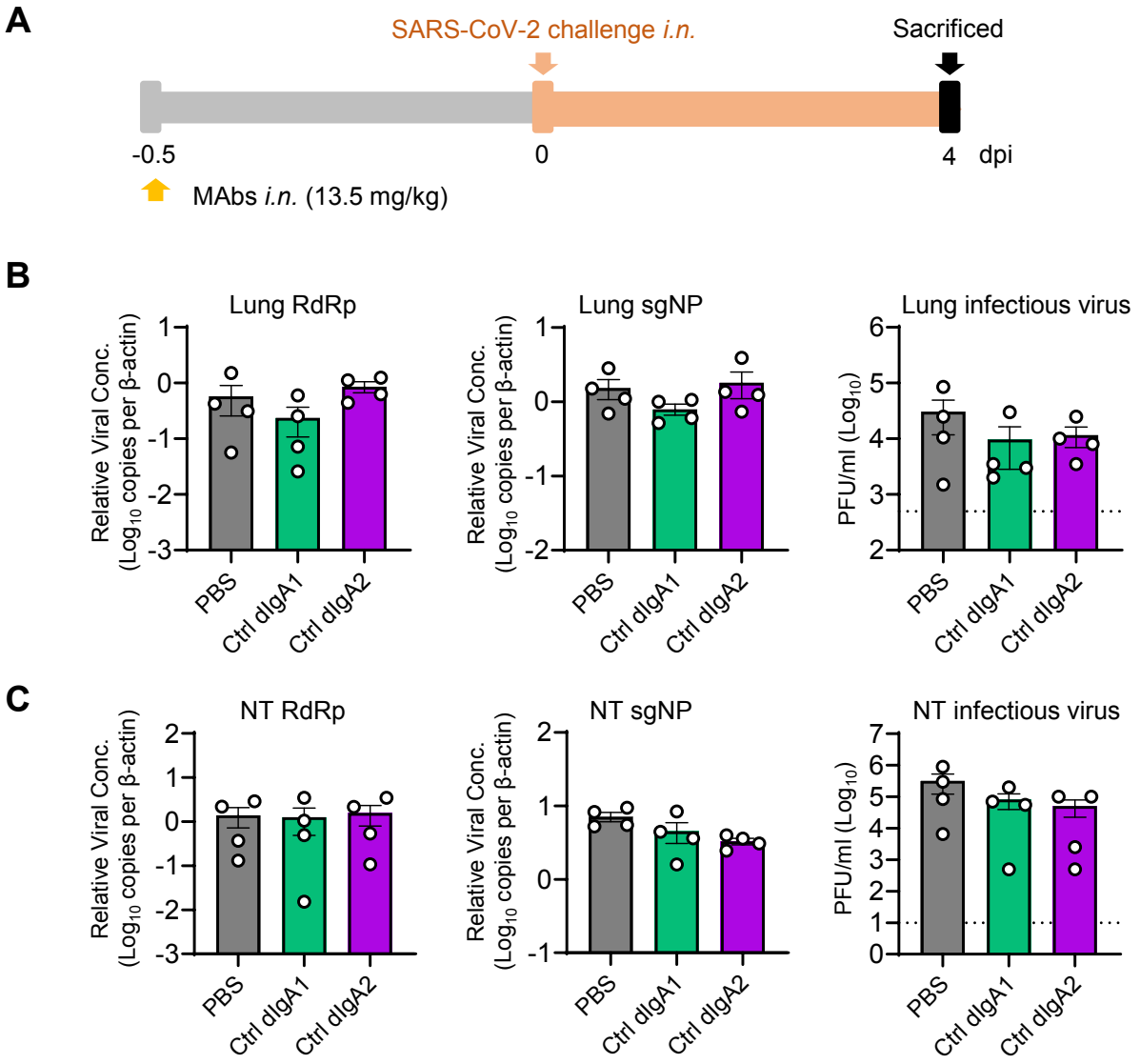

Supplementary Fig. 6. Control dIgA1 or dIgA2 did not mediate enhancement of SARS-CoV-2 infection in NT.

(A) Experiment schedule. Two groups of hamsters (n=4 per group) were inoculated intranasally with control dIgA1 and control dIgA2 at a high dose of 13.5 mg/kg 12 hours before intranasal viral challenge, respectively. Another group of hamsters (n=4) received PBS as control. On day 0, each hamster was intranasally challenged with a dose of 10^5 PFU of SARS-CoV-2 as mentioned in Figure 5A. All hamsters were sacrificed on 4 dpi for analysis.

(B) The viral loads in lung were determined by three assays.

(C) The viral loads in NT were determined by three assays.

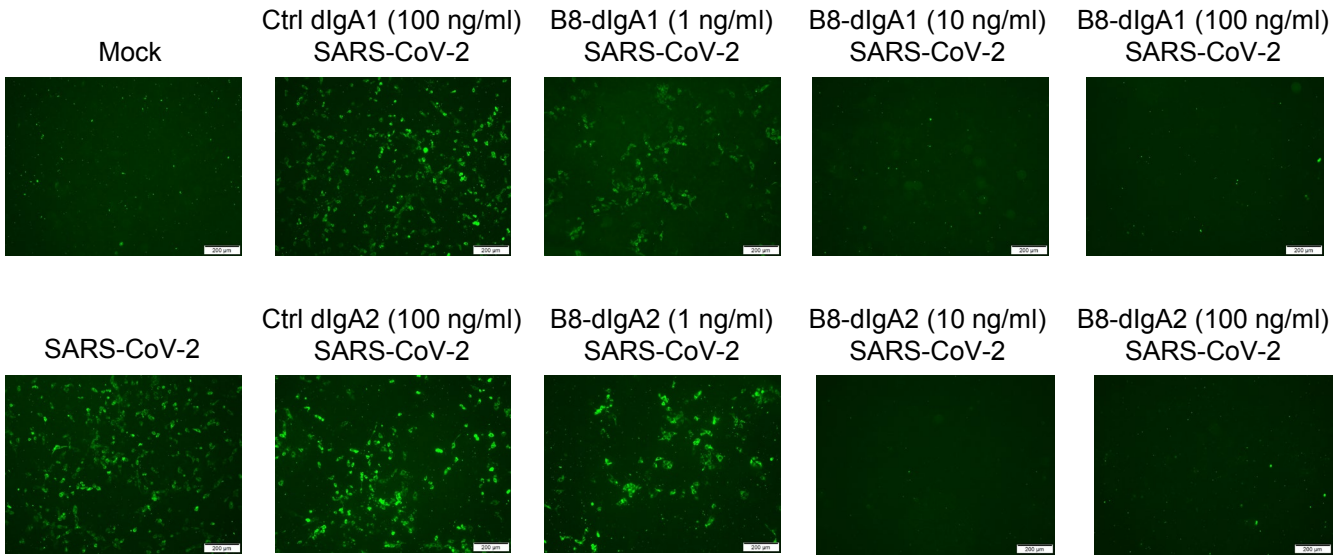

Supplementary Fig. 7. Potent neutralization of live SARS-CoV-2 infection by B8-dIgA1 and B8-IgA2 in human kidney cell line HK-2.

The IF staining of SARS-CoV-2 NP (in green) in infected HK-2 cells pre-treated with different dose of antibody as indicated. The representative image of each group was shown. Scale bars represent 200 μm.

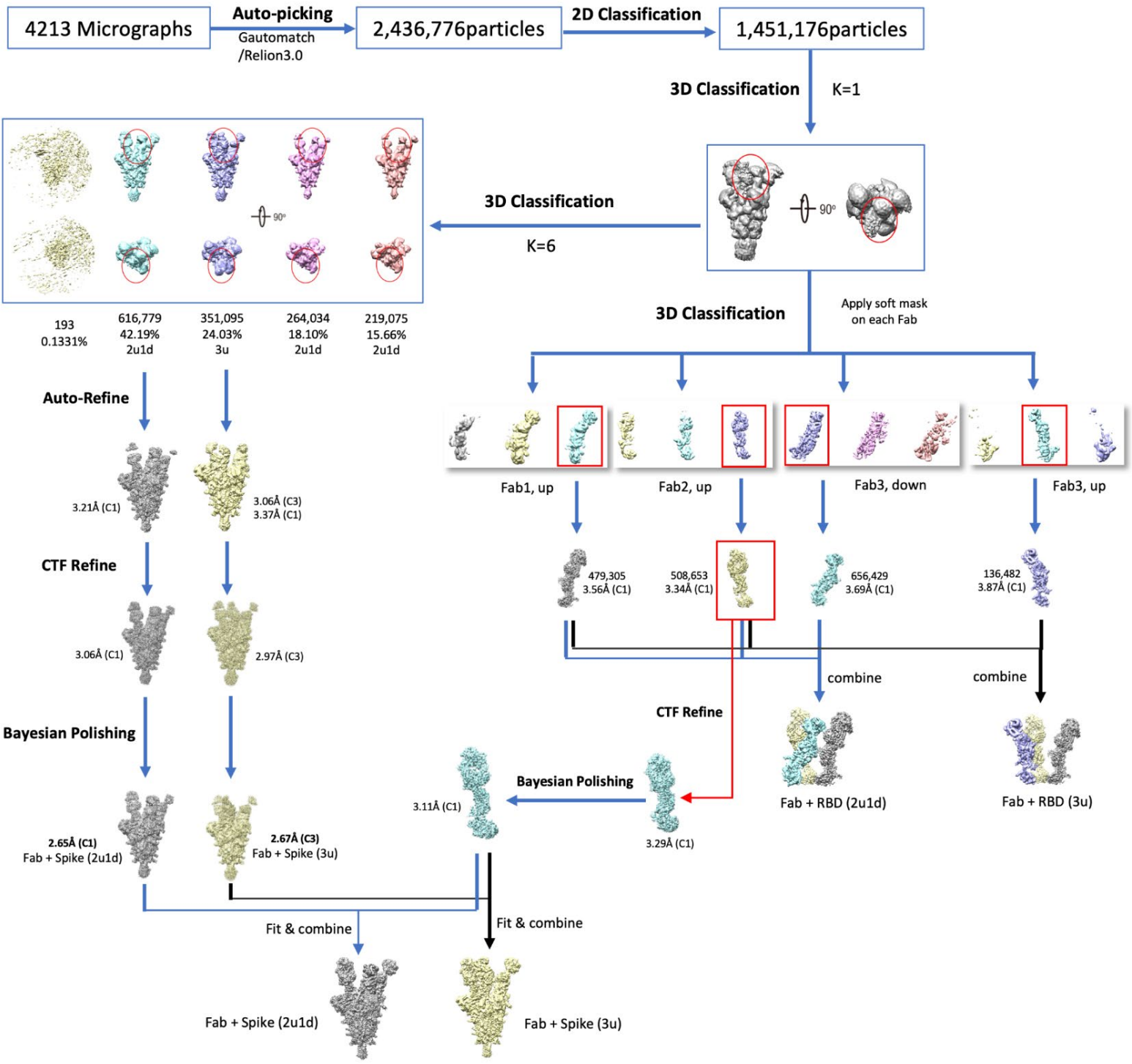

Supplementary Fig. 8. A flow-chart of SARS-CoV-2 S-B8 complex cryo-EM data processing. Different map density of RBD-Fab portions were emphasized in red cycle.

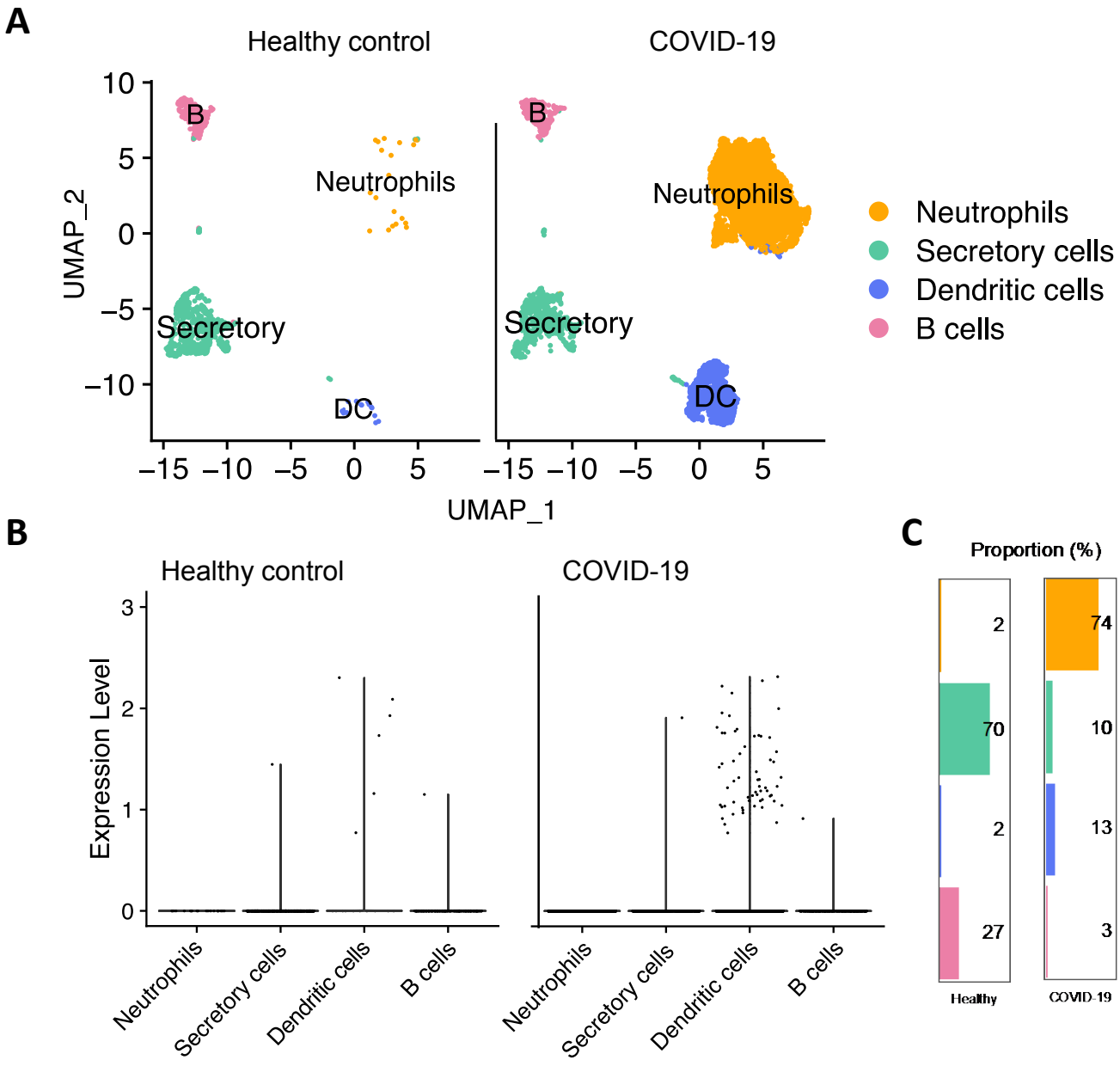

Supplementary Fig. 9. Preliminary analysis of the human nasal cytology data.
(A) The analysis was based data submitted under accession code GSE171488 (healthy donor nasal brushing) and GSE164547 (COVID-19 patient nasal brushing). Among CD14 positive cells, the neutrophil and monocyte-differentiated DCs were mainly increased in the nasal cytology samples of COVID-19 patients.
(B) Increased CD209 expression on nasal DCs of COVID-19 patients.
(C) The proportion of nasal DCs increased 6.5-fold from 2% to 13% in nasal samples compared between health and COVID-19 subjects.

Supplementary Table 1. Clinical characteristics of SARS-CoV-2 infected subjects.

Patient ID	Age	Gender	Days after symptom onset (or 1st hospitalization)	Disease Severity
P1	56	F	114	Severe
P2	62	M	116	Severe
P3	21	M	49	Asymptomatic
P4	75	M	15	Mild

Supplementary Table 2. Gene family analysis of four HuNAbs.

HuNAbs	Heavy chain				Light chain			
	IGHV	IGHJ	CDR3 length	SHM (%)	IGKV	IGKJ	CDR3 length	SHM (%)
B4	IGHV3-66*01, IGHV3-66*04	IGHJ6*02	12	3.8	IGKV1-33*01, IGKV1D-33*01	IGKJ5*01	9	4.6
B7	IGHV1-69*18	IGHJ6*02	18	0.0	IGKV3-11*01	IGKJ2*01	9	0.7
B8	IGHV1-69*18	IGHJ6*02	14	4.8	IGKV3-11*01	IGKJ4*01	9	1.7
C5	IGHV1-69*18	IGHJ4*02	16	2.4	IGKV3-20*01	IGKJ1*01	9	2.8

Supplementary Table 3. Binding ability of HuNAbs to SARS-CoV-2 RBD and spike.

HuNAbs	SARS-CoV-2 RBD	SARS-CoV-2 spike
	EC_{50} (μg/ml)	EC_{50} (μg/ml)
A6	0.30	17.94
B4	0.06	0.06
B7	0.04	0.018
B8	0.02	0.02
C5	0.03	0.03

Supplementary Table 4. Neutralization capability of RBD-specific HuNAbs.

HuNAbs	Pseudovirus		Live virus	
	IC_{50} (μg/ml)	IC_{90} (μg/ml)	IC_{50} (μg/ml)	IC_{90} (μg/ml)
B4	0.029	0.136	0.048	0.134
B7	0.015	0.094	0.030	0.060
B8	0.0095	0.046	0.013	0.032
C5	0.038	0.083	0.024	0.044

Supplementary Table 5. Surface plasmon resonance analysis of RBD-specific HuNAbs.

Antigen	Analyte	Kinetics model	ka (1/Ms)	kd (1/s)	KD (M)	tc
Spike	B4	1:1	2.11e+05	9.85e-05	4.66e-10	1.32e+13
Spike	B7	1:1	3.28e+05	4.35e-04	1.32e-09	2.08e+09
Spike	B8	1:1	2.24e+05	3.78e-05	1.69e-10	1.42e+12
Spike	C5	1:1	2.50e+05	7.70e-05	3.08e-10	1.56e+09

Supplementary Table 6. B8-IgG1 concentrations in different compartments of hamsters.

Group	Inoculation time (hour)	Inoculation dose (mg/Kg)	Day 0	Day 4		
			Serum (ng/ml)	Serum (ng/ml)	Lung homogenate (ng/ml)	Nasal turbinate homogenate (ng/ml)
G1	-24	*i.p.* 1.5	4257 ± 1517	2101 ± 1039	128.5 ± 13.18	20.66 ± 17.53
G2	24	*i.p.* 1.5	*N.A.*	4868 ± 797.8	238.1 ± 28.68	86.20 ± 18.73
G3	48	*i.p.* 1.5	*N.A.*	4135 ± 1674	229.3 ± 47.89	93.82 ± 8.302
G4	72	*i.p.* 1.5	*N.A.*	3252 ± 1749	192.4 ± 43.07	46.01 ± 3.934

N.A.: Not applicable

Supplementary Table 7. Binding of B8 HuNAbs to SARS-CoV-2 RBD and spike.

HuNAbs	SARS-CoV-2 RBD	SARS-CoV-2 Spike
	EC_{50} (μg/ml)	EC_{50} (μg/ml)
B8-IgG1	0.02	0.02
B8-mIgA1	0.020	0.006
B8-mIgA2	0.031	0.012
B8-dIgA1	0.019	0.011
B8-dIgA2	0.054	0.021

Supplementary Table 8. Neutralization potency of B8 HuNAbs.

HuNAbs	Pseudovirus		Live virus	
	IC_{50} (μg/ml)	IC_{90} (μg/ml)	IC_{50} (μg/ml)	IC_{90} (μg/ml)
B8-IgG1	0.0095	0.046	0.013	0.032
B8-mIgA1	0.012	0.052	0.012	0.018
B8-mIgA2	0.0057	0.014	0.010	0.051
B8-dIgA1	0.0048	0.033	0.015	0.026
B8-dIgA2	0.012	0.021	0.008	0.026

Supplementary Table 9. HuNAb concentration in different tissue compartments of infected hamsters.

HuNAbs	Inoculation time (hour)	Inoculation dose (mg/Kg)	Day 0	Day 4		
			Serum (ng/ml)	Serum (ng/ml)	Lung homogenate (ng/ml)	Nasal turbinate homogenate (ng/ml)
B8-mIgA1	-24	*i.n.* 4.5	90.71 ± 11.60	*U.D.*	16.54 ± 7.178	*U.D.*
	-24	*i.p.* 4.5	8682 ± 1749	*U.D.*	*U.D.*	*U.D.*
B8-mIgA2	-24	*i.n.* 4.5	21.36 ± 6.415	*U.D.*	*U.D.*	*U.D.*
	-24	*i.p.* 4.5	1561 ± 129.1	*U.D.*	*U.D.*	*U.D.*
B8-dIgA1	-12	*i.n.* 4.5	3.784 ± 2.081	*U.D.*	85.99 ± 17.52	*U.D.*
	-12	*i.n.* 13.5	1.981 ± 0.2688	*U.D.*	88.48 ± 23.44	*U.D.*
B8-dIgA2	-12	*i.n.* 4.5	*U.D.*	*U.D.*	6.383 ± 4.624	*U.D.*
	-12	*i.n.* 13.5	*U.D.*	*U.D.*	409.1 ± 108.0	*U.D.*

U.D.: undetectable

Supplementary Table 10. HuNAb concentration in different tissue compartments of naive Syrian hamsters at the time of viral challenge.

HuNAbs	Inoculation time (hour)	Inoculation dose (mg/Kg)	Day 0			
			Nasal wash (ng/ml)	Serum (ng/ml)	Lung homogenate (ng/ml)	Nasal turbinate homogenate (ng/ml)
B8-IgG1	-12	*i.n.* 4.5	208.6 ± 23.23	479.9 ± 62.53	24336 ± 2661	121.1 ± 26.38
B8-mIgA1	-12	*i.n.* 4.5	315.9 ± 186.1	18.84 ± 5.802	18914 ± 1672	53.87 ± 11.14
B8-mIgA2	-12	*i.n.* 4.5	204.1 ± 25.18	16.05 ± 2.515	32712 ± 12440	116.5 ± 72.62
B8-dIgA1	-12	*i.n.* 4.5	43.18 ± 27.52	6.827 ± 6.520	4347 ± 1598	14.74 ± 5.448
B8-dIgA2	-12	i.n. 4.5	56.79 ± 15.69	19.00 ± 7.562	28033 ± 12575	23.74 ± 1.445

Supplementary Table 11. Statistics of cryo-EM data collection, processing and model refinement.

Data collection						
EM equipment	Titan Krios					
Voltage (kV)	300					
Detector	K3 Summit					
Electron dose (e^{-}/Å^2)	50					
Defocus range (μm)	-1.0 ~ -2.0					
Pixel size (Å)	1.0979					
Reconstruction						
Software	Relion 3.0 & Relion 3.1					
Structure & state	Spike		RBD-Fab			
	3u	2u1d	#1, up	#2, up	#3,down	#3,up
Symmetry imposed	C3	C1	C1	C1	C1	C1
Final particles	616,779	351,095	479,305	508,653	656,429	136,482
Map resolution (Å)	2.76	2.65	3.56	3.11	3.69	3.87
Atomic modeling						
Software	Chimera, Coot, Phenix					
R.m.s. deviations						
Bond lengths (Å)	0.003	0.004	0.004	0.003	0.003	0.03
Bond angles (°)	0.591	0.601	0.815	0.683	0.628	0.794
MolProbity score	1.63	1.72	2.05	1.86	2.09	2.29
Clash score	5.36	6.32	9.99	7.21	12.05	17.48
Poor rotamers (%)	0	0	0	0	0.19	0
Ramachandran plot (%)						
Favored	95.15	94.55	90.66	92.5	91.69	90.24
Allowed	4.85	5.45	9.34	7.5	8.31	9.76
Outliers	0	0	0	0	0	0

Supplementary Table 12. Contacts between SARS-CoV-2 RBD and B8 Fab (distance cutoff 4Å).

RBD	Heavy chain	RBD	Light chain
V445	E1	E484	W94
G446*	K98	G485	W94
Y449*	N31, Y32, K98	F486*	N93, W94
N450	N31	N487*	N93
L452	N31, F55, L101	Y489*	S92, N93
F456*	L104	T500*	T56
T470	F55		
I472	T57		
V483	N59		
E484	R50, L52, T57, N59, F103		
C488	F103		
Y489*	F103, L104		
F490	F55, L101		
L492	L101, A102		
Q493*	A102, L104		
S494	N31, L101		

* ACE2 binding sites

Supplementary Table 13. Neutralization of SARS-CoV-2 variants by B8-derived HuNAbs.

Fold change of IC50 from WT (D614G)		RBD-specific HuNAb				
		B8-IgG1	B8-mIgA1	B8-dIgA1	B8-mIgA2	B8-dIgA2
UK (B.1.1.7)	UKΔ8	-30.4	-25.3	-6.5	-19	-22.5
	69-70del	-4.5	-0.2	-0.3	0.2	-1.5
	N501Y	-3.7	-3	-5	-2.3	-3.9
	A570D	0.4	0.6	0.5	-0.4	-0.5
	P681H	-0.1	0.7	0.5	0.5	0.6
	S982A	0.6	0.4	0.2	0.4	0
	D1118H	-4.8	-3.2	-2.3	-2.4	-3
SA (B.1.351)	SAΔ9	-71.7	<-1000	<-1000	-81.8	-549
	L18F	-5.6	-0.1	-0.1	-1.1	-0.9
	D80A	-4.5	-3.3	-1.3	-0.3	-0.9
	D215G	-22	-26.4	-11.5	-21.3	-15.3
	242-244 del	-5.2	-0.5	-3.2	-0.1	-0.9
	R246I	-2.4	-0.7	0.3	0.3	-0.4
	K417N	-1.7	0.5	0.3	-0.2	-1.9
	E484K	-779.5	<-1000	<-1000	<-1000	<-1000
	N501Y	-3.7	-3	-5	-2.3	-3.9
	A701V	-0.1	-0.4	0.3	0.7	0.4
Others	G485S	-1.3	-1.8	-2.1	0.7	-0.6
	F486A	-5.6	0.9	-1	0.5	-0.9
	T716I	-1.3	-3.5	-0.9	-13.1	-5
	Y453F	-0.6	-5.3	-2.3	-0.5	0.8

Note: red, resistant; green, sensitive